B. subtilis MutS2 splits stalled ribosomes into subunits without mRNA cleavage

Esther Park[1], Timur Mackens-Kiani[2], Rebekah Berhane[1], Hanna Esser[2], Chimeg Erdenebat[2], A. Maxwell Burroughs[3], Otto Berninghausen[2], L. Aravind[3], Roland Beckmann[2], Rachel Green[1,4], Allen R. Buskirk[1,*]

[1]Department of Molecular Biology and Genetics and [4]Howard Hughes Medical Institute, Johns Hopkins University School of Medicine, Baltimore, United States.

[2]Gene Center and Department of Biochemistry, University of Munich, Munich, Germany.

[3]Computational Biology Branch, Intramural Research Program, National Library of Medicine, National Institutes of Health, Bethesda, United States.

*To whom correspondence should be addressed: buskirk@jhmi.edu

Abstract

Stalled ribosomes are rescued by pathways that recycle the ribosome and target the nascent polypeptide for degradation. In *E. coli*, these pathways are triggered by ribosome collisions through recruitment of SmrB, a nuclease that cleaves the mRNA. In *B. subtilis*, the related protein MutS2 was recently implicated in ribosome rescue. Here we show that MutS2 is recruited to collisions by its SMR and KOW domains and reveal the interaction of these domains with collided ribosomes by cryo-EM. Using a combination of *in vivo* and *in vitro* approaches, we show that MutS2 uses its ABC ATPase activity to split ribosomes, targeting the nascent peptide for degradation by the ribosome quality control pathway. Notably, we see no evidence of mRNA cleavage by MutS2, nor does it promote ribosome rescue by tmRNA as SmrB cleavage does in *E. coli*. These findings clarify the biochemical and cellular roles of MutS2 in ribosome rescue in *B. subtilis* and raise questions about how these pathways function differently in various bacteria.

Introduction

In bacteria, translating ribosomes stall when they encounter problems with an mRNA template, such as nucleotides that are chemically damaged and therefore unreadable, or truncations of the mRNA that result in the loss of the stop codon[1,2]. Ribosomes also stall when elongation is slowed by low concentrations of aminoacyl-tRNA at clusters of rare codons or by specific peptide sequences that are difficult for the active site to accommodate (such as polyproline sequences)[3–6]. Indeed, certain arrest peptides such as SecM and TnaC take advantage of reversible ribosome stalling as a means to regulate the expression of downstream genes[7–10]. In addition, bacterial ribosomes are arrested by many antibiotics[11,12]. If left unresolved, ribosome stalling by any of these mechanisms can be dangerous to the cell because it reduces the pool of active ribosomes and leads to the production of truncated, potentially toxic proteins.

Over the course of evolution, these problems imposed selective pressure that favored the emergence of dedicated pathways that rescue stalled ribosomes. These pathways accomplish the twin tasks of recovering the ribosomes and targeting the truncated nascent peptides and problematic mRNAs for degradation[13]. The best characterized pathway in bacteria involves transfer-messenger RNA (tmRNA) which selectively rescues ribosomes stalled at the end of truncated mRNAs lacking a stop codon (so-called 'non-stop' messages)[14,15]. The ribosome resumes translation using tmRNA as a template, adding a peptide tag to the nascent polypeptide that targets it for degradation by proteases, primarily ClpXP[16]. Nearly all bacterial genomes encode tmRNA. There are also backup mechanisms that become engaged when tmRNA is overwhelmed. In *E. coli* and in *B. subtilis*, the backup pathway involves a small protein (ArfA/BrfA, respectively) that recruits a release factor to hydrolyze the nascent peptidyl-tRNA and promote recycling of the ribosome subunits without targeting the peptide for degradation[17–19]. Both of these pathways show a preference for ribosomes stalled on truncated mRNAs and require that the active site of the ribosome be competent to catalyze peptidyl transfer (for tmRNA) or peptidyl hydrolysis (for ArfA).

Several bacteria, including *B. subtilis*, also have a distinct pathway that shares similarities to the archaeo-eukaryotic pathway known as ribosome-associated quality control (RQC). In eukaryotes, stalled ribosomes are split into subunits, yielding a free small subunit and a large subunit with a trapped peptidyl-tRNA[20,21]. A factor called Rqc2 in yeast then catalyzes the addition of C-terminal Ala and Thr tails (CAT tails) to the nascent peptide, translocating the peptide out of the tunnel such that encoded Lys residues can be tagged with ubiquitin by Ltn1 and ultimately degraded by the proteasome[22–24]. In a similar fashion, *B. subtilis* contains a homolog of Rqc2 called RqcH which binds to dissociated 50S subunits with peptidyl-tRNA trapped on them and catalyzes the addition of Ala residues (Ala-tails) to the nascent peptide[25–27]. Like the tmRNA tag, these Ala-tails target the nascent peptide for degradation by the bacterial proteasome equivalent, ClpXP. Many questions remain regarding how the RQC pathway operates in bacteria including: (1) what are the natural substrates of this pathway and how they are recognized, (2) how are stalled ribosomes split in order to generate the 50S-peptidyl-tRNA substrate for RqcH and (3) how is the nascent peptide hydrolyzed from the tRNA and released.

We recently showed that ribosome rescue in *E. coli* is triggered by collisions that occur when a trailing ribosome catches up to a stalled ribosome[28]. The stable interaction between the two ribosomes (primarily through their 30S subunits) creates a new interface that recruits a factor called SmrB. This factor has an SMR domain that performs endonucleolytic cleavage of mRNAs when bound between collided ribosomes; cleavage occurs just upstream of the stalled ribosome. This cleavage in the ORF creates a non-stop mRNA such that upstream ribosomes that translate to this newly formed 3'-end are rapidly rescued by tmRNA. In addition to the cryo-EM structure of *E. coli* collided ribosomes bound to SmrB, we also reported the structure of collided ribosomes from *B. subtilis*, arguing that collisions are a conserved mechanism for recognizing stalled ribosomes in bacteria[29], much like in yeast and human cells[28,30–32].

Pfeffer and Joazeiro also reported the structure of collided ribosomes from *B. subtilis* bound to a factor homologous to SmrB called MutS2[33]. Like SmrB, MutS2 contains an SMR domain, but unlike SmrB it also contains several other domains including an ABC ATPase domain. The structure revealed that MutS2 binds to collided ribosomes as a dimer and that its ATPase domains contact the lead ribosome[33]. These observations raised the exciting possibility that MutS2 recognizes collided ribosomes specifically and uses its ATPase domain to split the stalled ribosomes into subunits. Thus, MutS2 could be the missing factor required to dissociate ribosomes to promote Ala-tailing by RqcH. It remained unclear, however, how MutS2 selectively binds collided ribosomes since the ATPase domains bind to the lead ribosome alone and the SMR domain was not resolved in their structure. Furthermore, these studies did not establish whether MutS2 cleaves mRNA using its SMR domain as we had observed with *E. coli* SmrB[33].

Here, we thoroughly characterize the role of MutS2 in ribosome rescue in *B. subtilis*. We show that MutS2 is recruited by ribosome collisions and report the cryo-EM structure of the SMR and KOW domains of MutS2 bound to collided ribosomes. We find that the SMR domain plays an important role in recruiting MutS2 to collided ribosomes. Using a reporter construct *in vivo*, we show that MutS2 uses its ATPase activity to split ribosomes into subunits, promoting Ala-tailing of the nascent peptide by RqcH. Importantly, we see no evidence of mRNA cleavage by MutS2, arguing that it does not act upstream of the tmRNA pathway as SmrB does in *E. coli*. Finally, we reconstitute the "rescue" reaction *in vitro* using purified collided ribosomes and show that MutS2 splits the stalled ribosomes into subunits in an ATP-dependent fashion but lacks detectable endonuclease activity. These findings define the biochemical activities of MutS2 in ribosome rescue in *B. subtilis*.

Results

Different architectures of bacterial SMR-domain proteins

SMR-domain proteins recognize ribosome collisions and cleave mRNA in *S. cerevisiae* (Cue2), *C. elegans* (NONU-1), and *E. coli* (SmrB) during ribosome rescue[28,34,35]. This study was prompted by our observation that SMR-domain proteins are broadly conserved in bacteria and cluster in three major clades with distinct domain architectures (Fig 1A,B). In *E. coli* and many other proteobacteria, the SMR domain is preceded by a relatively unstructured N-terminal extension,

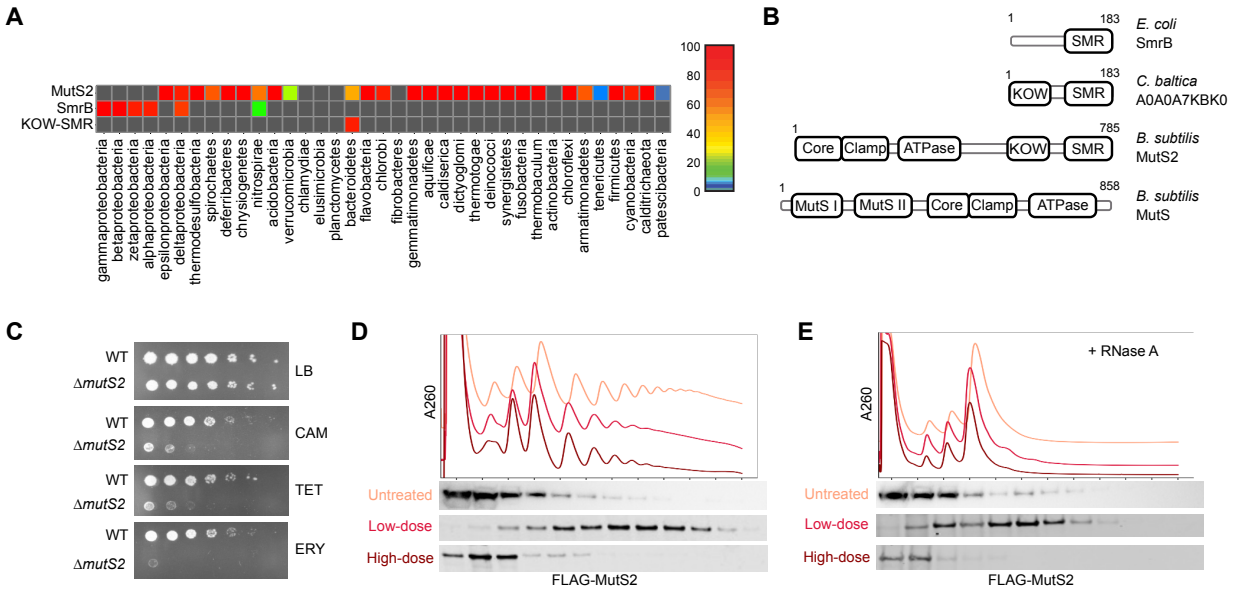

Figure 1. MutS2, an SMR domain protein in *B. subtilis*, binds collided ribosomes. (A) Heat map showing the percentage of genomes in each bacterial phylum encoding an SMR-domain protein. **(B)** Domain organization of three representative bacterial SMR-domain proteins and the related DNA mismatch repair factor MutS. **(C)** Spotting assay showing *ΔmutS2* cells are hypersensitive to chloramphenicol (CAM) (1 μg/mL), tetracycline (TET) (2 μg/mL), and erythromycin (ERY) (0.08 μg/mL). **(D)** Low doses of CAM induce collisions whereas high doses stall ribosomes without inducing collisions. Following treatment with low-does (2 μg/mL) and high-dose (200 μg/mL) CAM, the distribution of FLAG-MutS2 was determined by fractionation over sucrose gradients and detection with an anti-FLAG antibody. **(E)** Lysates from cells with and without CAM were treated with RNase A, fractionated over sucrose gradients, and the binding of FLAG-MutS2 to nuclease resistant disomes was detected with an anti-FLAG antibody.

as observed in SmrB (21 kD). Our previous structural and biochemical studies revealed that conserved residues in a helix in this extension (the N-terminal hook) bind to the ribosomal protein uS2 and play a key role in recruiting SmrB to ribosomes[28].

In contrast, the architecture most commonly found in other bacterial phyla is more complex, typified by the MutS2 protein in *B. subtilis* (87 kD). From N- to C-terminus, this architecture contains the core/lever, clamp, P-loop ABC ATPase, KOW, and SMR domains (Fig 1B). Notably, although the core/lever, clamp, and ATPase domains take their names from the homologous MutS protein involved in DNA mismatch repair[36], the MutS2 architecture lacks two N-terminal domains found in MutS, the MutSI (mismatch recognition) and MutSII (connector) domains. The absence of these two domains argues against MutS2 being involved in mismatch repair.

Finally, the third clade is the smallest, restricted to the bacteroidetes lineage. SMR domain proteins in this clade only have an N-terminal KOW domain and C-terminal SMR domain (e.g. *C. baltica*, Fig 1B), occasionally with an IG-like domain in between the two. Notably, some KOW domains in bacteria are known to have ribosome binding activity; for example, the KOW domain of NusG binds to ribosomal protein uS10[37], raising the possibility that the KOW domain in these two architectures (MutS2-like and KOW-SMR) plays a role in recruiting SMR-domain proteins to the ribosome.

Alignment of the SMR domains also revealed that residues previously implicated in mRNA cleavage are not equally conserved in these three clades. The DxH and GxG motifs in the SMR domain play a role in mRNA cleavage and RNA binding in *E. coli*[28], yeast[34], and plants[38]; these residues are highly conserved in SmrB proteins in proteobacteria and in the KOW-SMR protein in bacteroidetes. In contrast, we identified several independent occasions where the DxH active site residues have been wholly or partly lost in the MutS2 clade. An alignment of the SMR domain from MutS2 in firmicutes is shown in Fig. S1A. Many proteins have completely lost the DxH motif, whereas others such as MutS2 in *B. subtilis* have the residues DLR which do not conform to the consensus DxH motif. In firmicutes such as *B. subtilis*, the GxG motif is highly conserved, as is the His residue just upstream (residue His743 in *B. subtilis* MutS2). These observations raise questions about whether SMR domains in the MutS2 clade retain the endonucleolytic activity observed in *E. coli* SmrB.

ΔmutS2 cells are hypersensitive to antibiotics that target ribosomes

To explore whether the MutS2 protein in *B. subtilis* plays a role in translation, we first examined the phenotype of a strain lacking this factor. Δ*mutS2* cells did not have a significant growth defect compared to wild-type cells on plates made with rich medium. However, cells lacking MutS2 are hypersensitive to several antibiotics that target the ribosome. On plates with chloramphenicol (CAM), tetracycline (TET), or erythromycin (ERY), the growth of the Δ*mutS2* strain is less robust than wild-type (Fig 1C). In contrast, the Δ*mutS2* strain is not sensitive to beta-lactam antibiotics (e.g., carbenicillin) that target cell wall synthesis (Fig. S1B). These results suggest that MutS2 plays a role in mediating the toxicity of antibiotics that perturb the elongation stage of protein synthesis.

MutS2 preferentially binds collided ribosomes

We next asked whether MutS2 associates with ribosomes *in vivo*. To facilitate detection of MutS2, we ectopically expressed an N-terminally FLAG-tagged MutS2 construct from its native promoter in the Δ*mutS2* strain. We treated these cells with varying concentrations of chloramphenicol (CAM) to ask how ribosome collisions affect MutS2 binding to ribosomes. As shown previously in yeast and *E. coli*, high concentrations of antibiotics that target the ribosome stall ribosomes quickly in place, whereas lower doses only stall some ribosomes, allowing others to continue elongating until they collide with the stalled ribosomes[28,30]. We used this strategy to ask if MutS2 binds preferentially to collided ribosomes. In the untreated sample, MutS2 mostly is found in the light fractions of the sucrose gradient, although some portion is also found associated with monosomes and light polysomes, arguing that it can bind to ribosomes generally (Fig 1D). MutS2 is enriched in polysomes deeper in the gradient when cells were treated with a low dose of CAM (2 μg/mL), a concentration roughly equivalent to the minimum inhibitory concentration (MIC). Importantly, the enrichment of MutS2 in polysomes is lost in cells treated with much higher concentrations of CAM (200 μg/mL) (Fig 1D). We conclude that MutS2 weakly binds ribosomes in general and that its binding is enhanced by collisions, not merely by ribosome stalling.

We also asked whether MutS2 is preferentially recruited to nuclease-resistant disomes, a hallmark of collided ribosomes. Treatment of lysates with RNase A typically collapses most polysomes into monosomes, but when ribosomes have collided, RNase A cannot access the mRNA in the tight interface between them, thus leading to disome accumulation[31]. In untreated samples, polysomes collapsed into monosomes and MutS2 was mostly present in the lighter fractions (Fig 1E). However, in cells treated with 2 μg/mL CAM to induce collisions, small peaks corresponding to nuclease-resistant disomes and trisomes were identified; we observe that MutS2 is enriched in those deeper fractions (Fig 1E). As expected, in samples treated with high concentrations of CAM, MutS2 was not enriched in the heavier fractions.

The structure of the KOW and SMR domains of MutS2 on collided ribosomes

Cerullo *et al*. previously visualized MutS2 by cryo-electron microscopy as a homodimer bound to collided ribosomes[33]. Although their work beautifully reveals the overall arrangement of the lever, clamp, and ATPase domains of MutS2 on collided disomes, it does not provide insight into the positioning of the KOW and SMR domains in this interaction, nor does it reveal how colliding ribosomes are specifically recognized. In order to further elucidate the mechanisms of MutS2 recruitment and activity, we reconstituted the complex *in vitro*. Disomes from *B. subtilis* lysates were purified from an *in vitro* translation reaction of the MifM stalling construct as described previously[28,39]. A tenfold excess of purified MutS2 protein was added and the reaction was incubated in the presence of AMP-PNP. The sample was then vitrified and subjected to cryo-EM and single particle analysis.

3D classification of collided disomes selected from 2D classifications revealed two major classes: one with only mRNA density in the inter-ribosomal space and another with an additional density next to the mRNA (Fig 2A,B). The latter class also contained additional density next to uS10 on both the stalled and the collided ribosomes. By local refinement of the experimental data and rigid body-fitting of a model of MutS2 generated in Alphafold2[40], we identified these extra densities as the SMR and KOW domains, respectively (Fig 2B). Notably, in our structures we were not able to visualize the N-terminal domains seen in the previous structure (lever, clamp, and ATPase), perhaps due to differences in how the complexes were prepared.

The overall assembly of the collided disome with the MutS2 KOW and SMR domains is shown in Fig 2C. Only one of the SMR domains in the homodimer is visible, bound next to the mRNA in the inter-ribosomal space, interacting with both ribosomes (Fig 2D). In this position, the region of the SMR domain containing the DLR and GxG residues is oriented towards the mRNA, suggesting a specific interaction as observed for SmrB in *E. coli* (Fig 2F,G). On the stalled ribosome, the SMR domain interacts with uS11 and uS7, as previously reported for SmrB; on the collided ribosome, the SMR domain is positioned next to uS3. Curiously, unlike Cerullo *et al*., we do not observe bS21 in the stalled ribosome in our structure (Fig S2E,F).

The binding mode of the KOW domain is highly similar to that of NusG, an *E. coli* protein involved in transcription-translation coupling; both bind to uS10 with their KOW domain through similar interfaces[37]. We also observe partial density corresponding to the loop connecting the KOW and

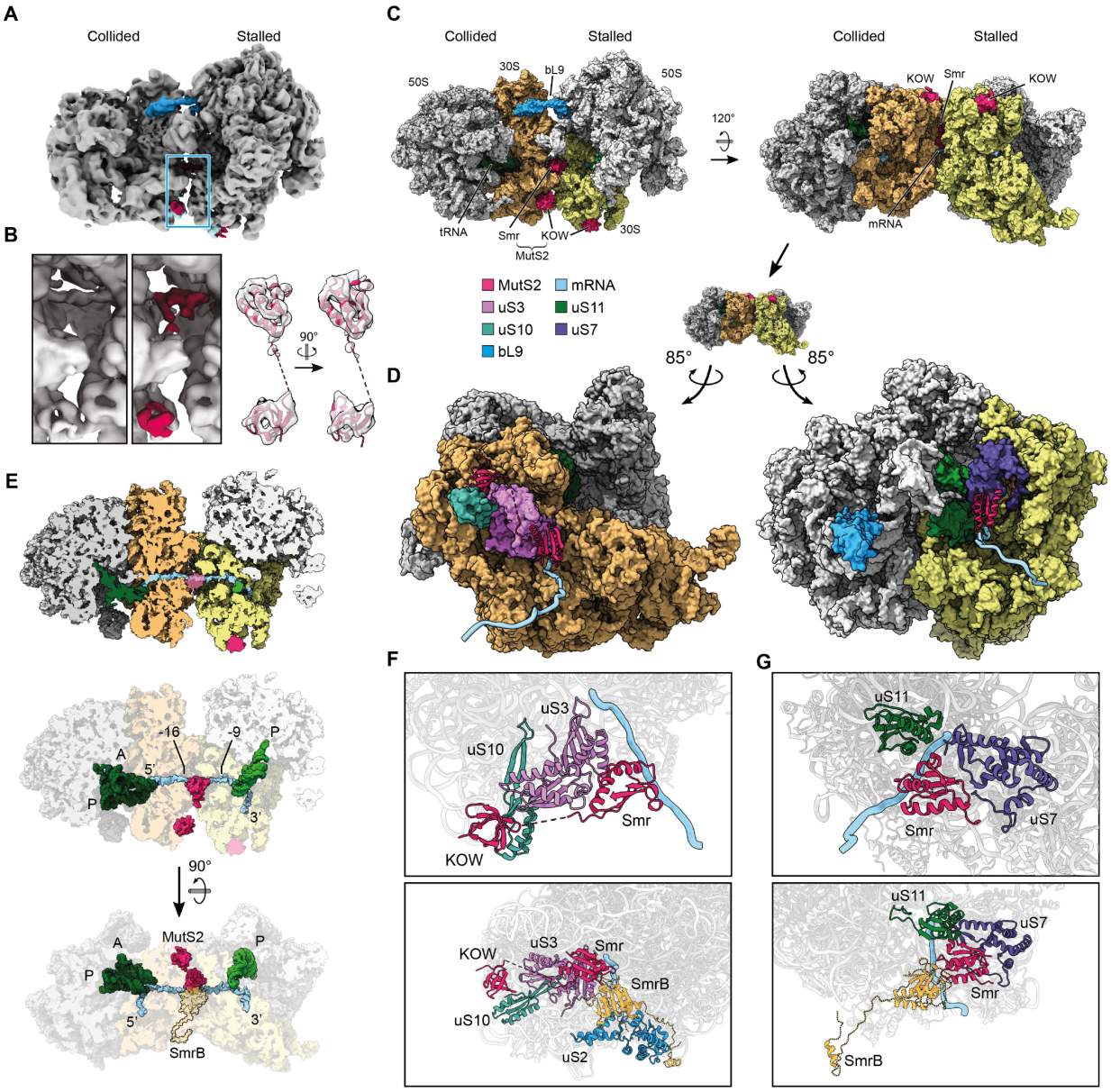

Figure 2. Cryo-EM structure of the MutS2 KOW and SMR domains binding the *B. subtilis* disome. (A) Experimental cryo-EM reconstruction, lowpass-filtered, with MutS2 in red, uS10 in light blue, and uL9 in blue. **(B)** Left: Zoomed-in view of the inter-ribosomal interface of a class of particles without (left) and with (right) MutS2. Right: Fit of the MutS2 KOW and SMR domains into the experimental density. **(C)** Cryo-EM structure of the collided *B. subtilis* disome bound by the MutS2 KOW and SMR domains. **(D)** Interactions of MutS2 with the collided disome interface, seen from each side of that interface. **(E)** Top, Middle: Cut view of the MutS2-bound disome showing the mRNA path and the position of the KOW and SMR domains as well as tRNA (green) in both ribosomes. Bottom: Comparison of the position of MutS2 in the *B. subtilis* disome to that of SmrB in the *E. coli* disome. **(F)** Top: Close-up view of the interactions of MutS2 on the collided ribosome-side of the interface. Bottom: Comparison of the same with the conformation of a hypothetical *E. coli* SmrB binding to the same disome structure. **(G)** Top: Close-up view of the interactions of MutS2 on the stalled ribosome-side of the interface. Bottom: Comparison of the same with the conformation of a hypothetical *E. coli* SmrB binding to the same disome structure.

ribosome belongs to the same MutS2 monomer as the observed SMR domain, whereas the KOW domain binding the stalled ribosome is part of a second copy of MutS2. The position of both KOW domains is compatible with the position of the coiled-coil domains of the MutS2 dimer observed by Cerullo *et al*.[33]; no structural rearrangements would be required to link the density of the N-terminal domains in the previous structure with the C-terminal domains reported here (Fig S2A-C).

Finally, although the SMR domains of both MutS2 and SmrB recognize composite binding sites formed between the collided ribosomes near the bridging mRNA, the orientation of the SMR domain is very different in the two complexes from *B. subtilis* and *E. coli*. This difference in the SMR domain orientation may arise from constraints imposed by additional interactions of the N-terminal hook of SmrB with uS2 and by the MutS2-KOW domain with uS10. As a result, compared to SmrB, the SMR domain of MutS2 is rotated around the mRNA by approximately 120° (Fig 2E). Together with the lack of amino acid conservation, this finding raises the question whether the SMR domain of MutS2 possesses the same catalytic activity as an endonuclease as documented for SmrB[28].

MutS2 releases truncated proteins from stalled ribosomes but does not affect mRNA levels

To study the activity of MutS2 *in vivo*, we designed reporter constructs that allow us to follow the translation of a problematic mRNA in *B. subtilis* (Fig 3A). Each reporter contains an in-frame fusion of NanoLuc to the bleomycin resistance protein (BleR). We created two control constructs, one with a stop codon between the genes that produces NanoLuc alone (Stop) and a second without any stalling motif (Non-stall) that produces the full-length fusion protein. In a third construct, we inserted the 31-residue ApdA stalling motif between NanoLuc and BleR (ApdA). This arrest peptide from *A. japonica* arrests elongating *B. subtilis* ribosomes by inhibiting peptidyl transfer[41].

To confirm that ribosome stalling at ApdA triggers downstream rescue pathways, we performed a western blot using antibodies against NanoLuc. A strong band corresponding to full-length protein is observed for the Non-stall control and loss of MutS2 did not affect this reporter, as expected (Fig 3B). In contrast, there is significantly less full-length protein for the ApdA reporter because stalling lowers the protein output. Moreover, the ApdA reporter generates a truncated protein that is slightly larger than the NanoLuc produced from the Stop control, consistent with translation of the additional ApdA sequence prior to ribosome stalling. Importantly, the loss of MutS2 resulted in a substantial decrease in the amount of truncated reporter protein from the ApdA reporter (Fig 3B). These results are consistent with a model wherein MutS2 rescues ribosomes stalled in the middle of an open reading frame (ORF) thus releasing truncated protein products.

In addition, we analyzed the activity of MutS2 on the reporter mRNA using northern probes specific for the 5'- or 3'-ends (Fig 3C). With the 5'-probe, we see primarily full-length mRNA from the Non-stall reporter. Remarkably, there appears to be similar levels of full-length mRNA from the ApdA reporter as well, in stark contrast to our previous observation in *E. coli* that the

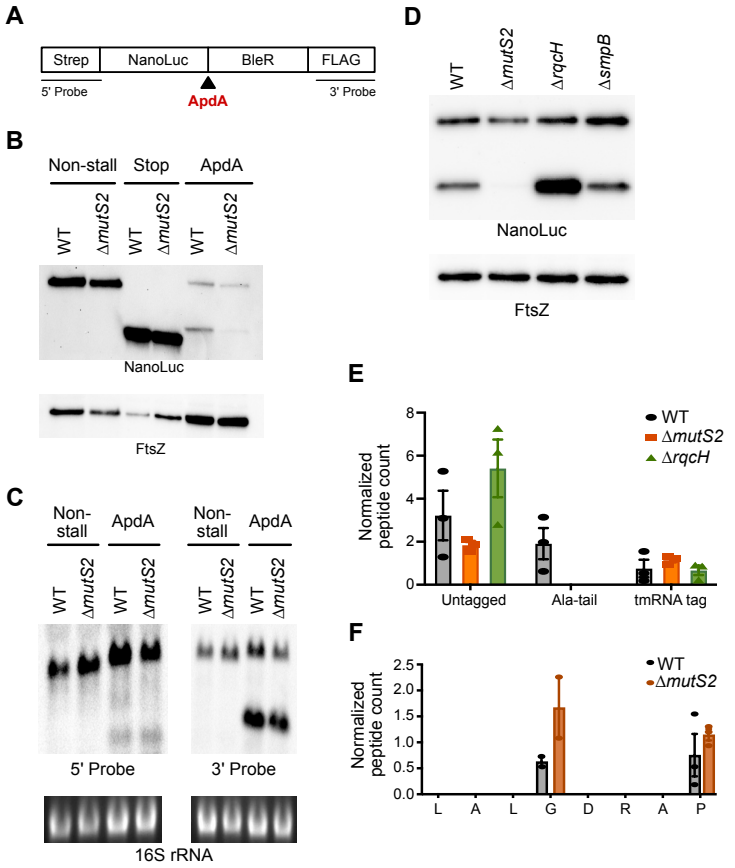

Figure 3. MutS2 rescues ribosomes stalled in the middle of an ORF. (A) Schematic of stalling reporter for studying ribosome rescue in *B. subtilis*. Between the NanoLuc gene and bleomycin resistance gene, we inserted either no additional sequence (Non-stall), stop codons (Stop), or the ApdA stalling motif. **(B)** Reporter protein from wild-type and *ΔmutS2* strains was detected by anti-NanoLuc antibodies. The FtsZ protein serves as a loading control. **(C)** Northern blots of reporter mRNA using the 5'-probe and the 3'-probe. Ethidium bromide staining of the 16S rRNA serves as a loading control. **(D)** Reporter protein from wild-type, *ΔmutS2*, *ΔrqcH*, and *ΔsmpB* strains was detected by anti-NanoLuc antibodies. The FtsZ protein serves as a loading control. **(E)** Addition of the tmRNA tag or the Ala-tail at the stall site of the reporter in wild-type, *ΔmutS2*, and *ΔrqcH* strains was detected by LC-MS/MS. The peptide counts are normalized to a different peptide in the reporter protein. **(F)** tmRNA tagging along the stalling sequence in wild-type and *ΔmutS2* strains showing that tmRNA tagging is not dependent on MutS2.

presence of a strong arrest peptide dramatically lowers full-length reporter mRNA levels[28]. This finding suggests that unlike in *E. coli*, where ribosome stalling targets transcripts for decay by SmrB nuclease activity, ribosome stalling does not target the reporter mRNA for decay in *B. subtilis*. With the 3'-probe, again we see that full-length mRNA levels are similar with or without the ApdA stalling sequence. With this probe, we also detect a decay intermediate from the ApdA reporter corresponding to the mRNA fragment downstream of the stall site; importantly, loss of MutS2 does not affect the level of this fragment, suggesting that MutS2 is not responsible for its production. We speculate that the truncated band arises from degradation of the upstream mRNA by the 5'-3' exonucleases until they are blocked by the stalled ribosome, yielding a stable, downstream fragment[42]. Taken together, these data show that MutS2 generates a truncated protein product from ribosomes stalled in the middle of an ORF but does not affect mRNA levels, suggesting that, unlike SmrB, it may indeed lack nuclease activity.

Ala-tailing by RqcH depends on MutS2

We envisioned that MutS2 might release truncated proteins from stalled ribosomes in two different ways, depending on the activity of the protein; these possibilities are not mutually exclusive. First, if MutS2 were to cleave the mRNA on collided ribosomes, then upstream ribosomes would arrest at the newly formed 3'-end and be rescued by tmRNA, leading to the release of truncated protein with C-terminal SsrA tags encoded by tmRNA during the rescue

process. Typically, SsrA-tagged proteins are rapidly degraded by the ClpXP protease[43]. If the tmRNA system is overwhelmed, however, a backup system involving ArfA in *E. coli* or BrfA in *B. subtilis* typically releases the nascent peptide without adding a degron tag[17–19]. In *E. coli*, we previously observed that cells lacking tmRNA generate far higher levels of truncated protein products from a stalling reporter because the ArfA-released (and therefore untagged) protein products are stable relative to those that were tagged by tmRNA[28]. We find that in *B. subtilis* cells in which the tmRNA pathway was inactivated by deletion of its protein partner SmpB, there is no difference in the level of truncated protein produced compared to the wild-type cells (Fig 3D); thus, there is no major role for the tmRNA system in resolving the stalled ribosomes on ApdA. This finding is consistent with the lack of evidence that MutS2 cleaves the reporter mRNA to generate a prototypical non-stop message substrate for tmRNA/SmpB.

A second possible mechanism of action is that the ATPase domain of MutS2 splits the stalled ribosome into subunits, freeing the 30S subunit but yielding a 50S subunit with peptidyl-tRNA trapped on it, akin to the activity of RQT in eukaryotic systems[20]. It has been shown that in *B. subtilis* (as in eukaryotes) the 50S-peptidyl-tRNA complex is a substrate for the RQC factor RqcH which adds several Ala residues to the C-terminus of the nascent polypeptide and targets the protein for degradation by ClpXP[25–27]. In this case, the expectation would be that deletion of RqcH should stabilize truncated proteins produced by this pathway because they would not be Ala-tailed[25]. Indeed, we observe higher levels of truncated protein from the reporter construct in the absence of RqcH (Fig 3D), consistent with the model proposed by Cerullo *et al*. in which MutS2 splits ribosomes into subunits that are then acted on by RqcH to target the nascent peptide for degradation[33].

To further characterize the truncated protein, we used mass spectrometry to identify C-terminal fragments to detect whether SsrA-tag or Ala-tails were added during the rescue process. We grew cells with bortezomib (an inhibitor of ClpXP) to prevent degradation of the truncated proteins and immunoprecipitated the ApdA reporter protein from wild-type, *ΔmutS2*, and *ΔrqcH* strains. We then digested the protein with lysyl endopeptidase and subjected the resulting peptides to liquid chromatography with tandem mass spectrometry (LC-MS/MS). Ribosomes stall near the end of the ApdA sequence at the RAPP motif with the first Pro codon in the P site and the second Pro codon in the A site[41]. We observed abundant peptides in all three strains ending in RAP (Fig 3E). These represent proteins unmodified by tmRNA or RqcH possibly arising from peptides released from the 50S after splitting (without Ala-tails) or nascent peptides on 70S ribosomes released from tRNA during sample preparation. More interestingly, we observe peptides with alanine-tails added at the site of the stall (after RAP). These peptides are only observed in the wild-type strain. Deletion of RqcH leads to loss of Ala-tailing, as expected, and likewise, deletion of MutS2 similarly leads to loss of Ala-tailing (Fig. 3E). These findings are consistent with a model wherein MutS2 activity is upstream of Ala-tailing by RqcH *in vivo*. Indeed, based on their observations of loss of Ala-tagging in strains lacking MutS2, Cerullo *et al*. proposed renaming MutS2 as RqcU (RQC-upstream factor)[33].

We also observed proteins that had been tagged by tmRNA. These peptides were less abundant than those released at the stall site (ending in RAP) or those with Ala-tails, although with the

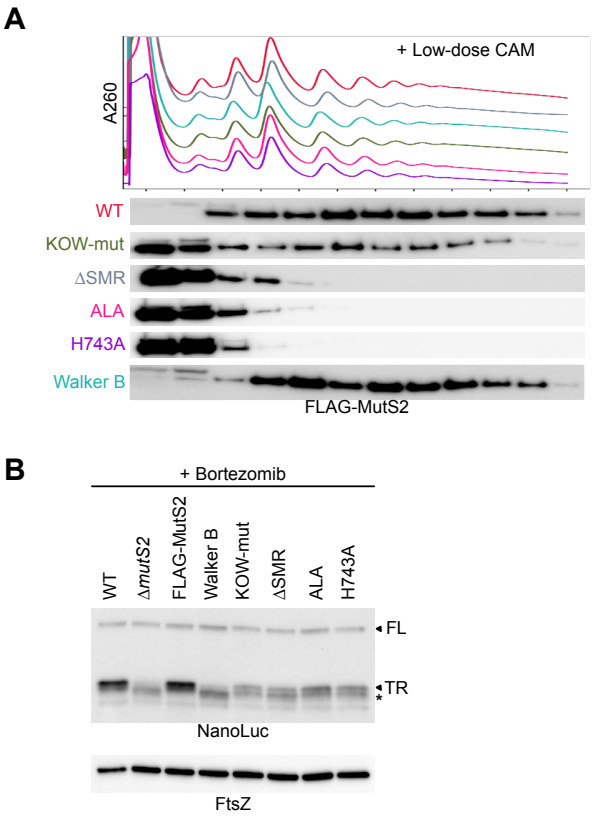

Figure 4. Activities of the SMR and ATPase domains of MutS2. **(A)** Following induction of ribosome collisions with CAM, the distribution of Flag-tagged MutS2 and several mutants was determined by fractionation over sucrose gradients and detection with anti-FLAG antibody. ΔSMR is missing the SMR domain (residues 710-785). The Walker B mutant prevents ATP hydrolysis (E416A). KOW-mut contains mutations to the KOW domain to perturb binding to S10 (QxxILK to AxxAAA). ALA and H743A are mutations to conserved residues in the SMR domain. **(B)** Cells expressing various constructs of MutS2 were grown with 20 μM bortezomib to inhibit ClpXP activity and reporter protein was visualized using an anti-NanoLuc antibody. FL = full-length ApdA reporter protein, TR = truncated reporter protein, * = smaller truncated protein not dependent on MutS2 activity. The FtsZ protein serves as a loading control. **(C)** Spotting assay of strains expressing various MutS2 constructs on plates with and without erythromycin (0.08 μg/mL).

challenges in mass spectrometry in detecting various peptides we cannot make any strong quantitative conclusions. The tmRNA tag is added to peptides right at the stall site after the RAP motif (Fig 3F) as well as at a second site after the Gly residue four residues upstream. In both cases, the number of tmRNA tagged peptides was not reduced in samples prepared from cells lacking MutS2, arguing that MutS2 is not functioning upstream of tmRNA tagging at either site. We argue that tmRNA tagging arises from mRNA decay pathways unrelated to MutS2 in *B. subtilis*. These data are in stark contrast to our earlier observations in *E. coli* where tmRNA tagged products arising from upstream of the stall site disappear when SmrB is deleted[28]. Taken together, these data are consistent with a role for MutS2 in splitting the downstream ribosome into subunits (leading to Ala-tailing by RqcH) but do not provide evidence in support of mRNA cleavage by MutS2.

The KOW and SMR domains promote MutS2 binding to collided ribosomes

With insights from the cryo-EM structure, we next made a series of MutS2 mutations to determine how each domain contributes to binding collided ribosomes *in vivo*. Mutant FLAG-tagged MutS2 constructs were expressed from an ectopic site in the *ΔmutS2* strain; the expression levels of all the mutants were found to be roughly equivalent (Fig S3). We treated cultures with a low dose of CAM to induce collisions and performed western blots using anti-FLAG antibodies to follow MutS2 sedimentation across sucrose gradients.

Given that our structure revealed that the KOW domain binds to ribosomal protein uS10, we made several Ala mutations in a single construct designed to perturb the binding interface (KOW-mut), including Q668A, I671A,

L672A, and K673A. These surface-exposed residues lie in a loop corresponding to the conserved F165 in the KOW domain of NusG that is critical for ribosome binding[37]. As expected, binding of the KOW-mut protein is reduced compared to the wild-type (Fig. 4A); there is more protein in the first fractions and less bound to ribosomes deeper in the gradient.

The fact that the SMR domain is buried between the collided ribosomes suggests that it may specifically sense collisions through recognition of a distinct composite binding interface. Indeed, deletion of the SMR domain (ΔSMR) through truncation after residue 701 dramatically reduces MutS2 binding to ribosomes (Fig 4A). We also made mutations to conserved residues in the SMR domain likely to be involved in RNA binding, independently changing D_{711}LR to ALA and mutating the conserved His just upstream of the GxG motif (H743A). Both the ALA mutant and the H743A mutant show dramatic reductions in binding to colliding ribosomes (Fig. 4A). In contrast, we found that mutation of the Walker B motif (E416A) in the ATPase domain had little or no effect; this mutant still shifts deep into polysomes when collisions are induced (Fig. 4A). These results with the MutS2 mutants show that, consistent with our cryo-EM structure, the KOW and especially the SMR domain promote MutS2 binding to collided ribosomes.

The ABC-ATPase domain is critical for MutS2 function

To determine the effect of these mutations on the activity of MutS2, we introduced the ApdA stalling reporter into strains carrying the MutS2 mutants. We added bortezomib to cultures to prevent degradation of the truncated protein and performed western blots against NanoLuc, the upstream part of the stalling reporter. In wild-type cells, there is a strong band corresponding to the truncated reporter that is stabilized relative to the full-length protein by the addition of bortezomib (Fig. 4B) compared to untreated samples (Fig. 3B). There is also a band just below the major band that is not dependent on MutS2; in the *ΔmutS2* strain, only the top band decreases (TR), not the lower band (*). When a Flag-tagged copy of wild-type MutS2 is added to complement the deletion, the upper band is rescued to wild-type levels, indicating that the Flag-tag does not impact MutS2 activity.

The Walker B mutant yields little or no truncated MutS2 product (the upper band, TR), similar to the complete knockout strain, *ΔmutS2* (Fig 4B); these data indicate that inhibiting ATP hydrolysis abrogates MutS2 activity. In contrast, mutation of the KOW domain (KOW-mut) or the SMR domain (ΔSMR, ALA, H743A) yielded an intermediate phenotype, where we saw some reduction in the level of the upper band, but not a complete loss of MutS2 product. This loss of activity is likely due to the reduction in binding observed in Fig. 4A.

We also tested the effects of MutS2 mutations on the ability of cells to survive on plates with the collision-inducing antibiotic erythromycin (ERY). Just as *B. subtilis* cells lacking MutS2 are sensitive to ERY, so too are cells expressing the Walker B mutant (Fig 4C). In contrast, cells expressing the KOW-mut or mutations in the SMR domain showed only very modest sensitivity to ERY. These results show that the ATPase domain of MutS2 is associated with its most critical functional domain.

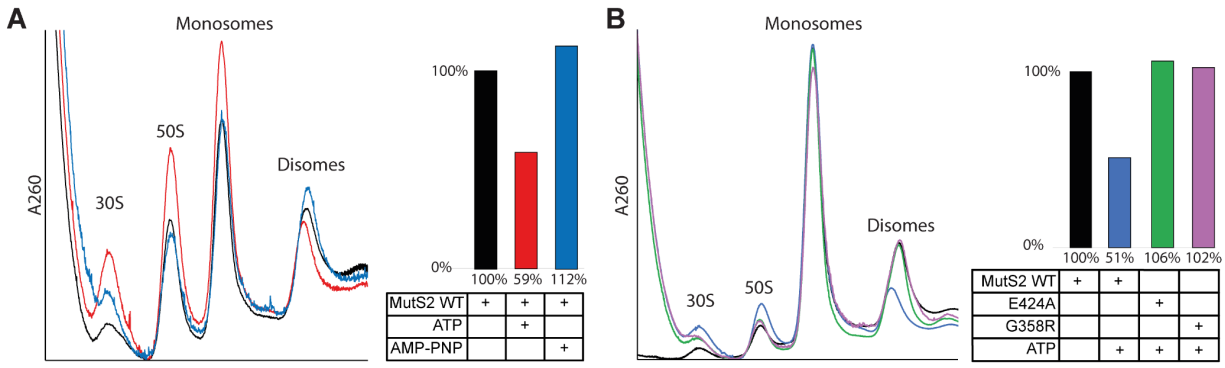

Figure 5. MutS2 splits stalled ribosomes into subunits *in vitro*. (A) Left: UV chromatograms from sucrose gradient fractionation of disome splitting assays with MutS2 WT. Right: Relative abundance of disomes compared to total ribosomal fractions after splitting reaction in experiments with MutS2 WT, calculated from relative peak areas in the chromatograms. Purified *B. subtilis* disomes were used as input. Only in the presence of ATP do we observe a significant decrease in the abundance of disomes compared to other ribosomal fractions after incubation with MutS2. **(B)** Left: UV chromatograms from sucrose gradient fractionation of disome splitting assays with MutS2 WT and ATPase (E424A: Walker B, G358R: Walker A) mutants. Right: Relative abundance of disomes compared to total ribosomal fractions after splitting reaction in experiments with MutS2 WT and ATPase mutants, calculated from relative peak areas in the chromatograms. Purified *B. subtilis* disomes were used as input. Mutations that render either the Walker A or Walker B domains non-functional abrogate the disome splitting activity of MutS2 entirely.

MutS2 splits disomes into ribosome subunits in vitro

We reconstituted disome splitting *in vitro*, purifying *B. subtilis* disomes from an *in vitro* translation reaction and combining them with purified wild-type or mutant MutS2. The reactions were then fractionated on a sucrose gradient in order to analyze the relative abundance of the remaining disomes, monosomes, and ribosome subunits, in order to determine the splitting efficiency.

When incubating the collided disomes with wild-type MutS2 in the presence of ATP, we generally observed a marked decrease in the disome peak compared to a control experiment in the absence of ATP. At the same time, we observed an increase in peaks corresponding to ribosomal subunits and monosomes, indicating disome splitting activity by MutS2 (Fig 5A, red). In these experiments, the contribution of the disome peak area to the total for all ribosomal fractions decreased by at least 40%. However, when ATP was substituted with the non-hydrolyzable analog AMP-PNP, no such decrease was observed, confirming that ATP hydrolysis is required for MutS2 splitting activity and that ATP binding alone is not sufficient (Fig 5A). We also found that the Walker A and Walker B mutants of MutS2 fail to split the disomes, even in the presence of ATP (Fig 5B); these data establish that ATP binding followed by hydrolysis by the MutS2 ATPase domain is required for efficient dissociation of disomes *in vitro*. In contrast, repeating the experiment with the MutS2 ALA mutant, which disrupts the DLR motif of the SMR domain, yielded similar splitting activity when comparing the SMR domain mutant with wild-type MutS2 (Fig S4). These data further argue that these residues in the SMR domain of MutS2 are not essential for disome splitting and that MutS2 does not carry out an endonuclease function.

Discussion

The data presented here support a model in which *B. subtilis* MutS2 promotes the rescue of stalled ribosomes in a dramatically different manner from *E. coli* SmrB (Fig 6). Although both proteins contain an SMR domain that recognizes the interface formed by two colliding ribosomes, helping to recruit them to their disome substrate, the biochemical activities of the two proteins are distinct. The SMR domain in SmrB functions as an endonuclease, cleaving mRNA between the collided ribosomes, allowing upstream ribosomes to translate to the newly formed 3'-end, where they are rapidly rescued by tmRNA. After canonical release and recycling on the tmRNA template, the tag encoded by tmRNA leads to degradation of the nascent peptide by proteases[28]. In contrast, the SMR domain in *B. subtilis* MutS2 is not an active nuclease, nor does it target ribosomes for rescue by tmRNA. Instead, the ATPase domain of MutS2 splits the stalled ribosomes into subunits, freeing the 30S subunit as well as a 50S subunit bound to peptidyl-tRNA. RqcH then facilitates the non-templated addition of Ala residues to the C-terminus of the nascent peptide, and after the peptide is released from the tRNA through an unknown mechanism, the Ala-tail targets it for degradation by proteases. Through these distinct mechanisms, both SmrB and MutS2 trigger pathways that recycle the stalled ribosomes and degrade the aborted nascent polypeptides.

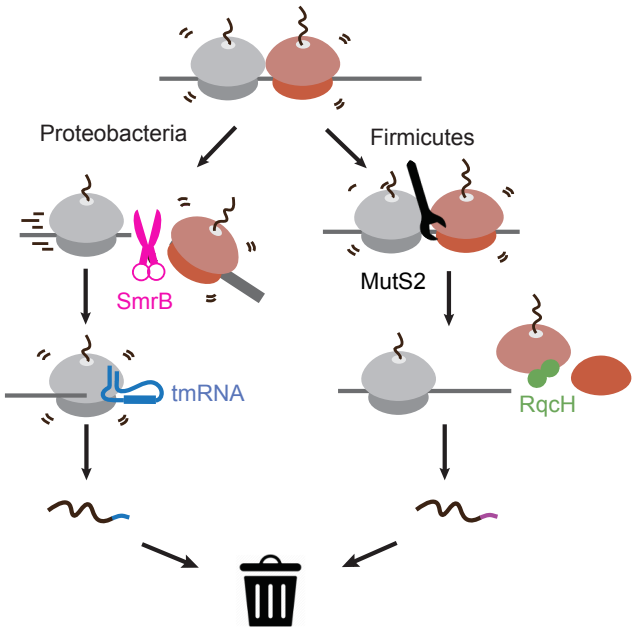

Figure 6. Model for ribosome rescue in bacteria. Proteobacteria containing SmrB rescue collided ribosomes via nucleolytic cleavage while firmicutes and other bacteria containing MutS2 split collided ribosomes into subunits. These differences mean that different pathways (tmRNA or RqcH) tag the nascent polypeptide to target it for degradation by proteases.

In this study, we clarify MutS2's mechanism of action in recognizing collided ribosomes in *B. subtilis*. Ribosome collisions are present in diverse bacteria and share common features. In *E. coli* and in *B. subtilis*, the SMR domain plays a role in recruiting both SmrB and MutS2 to collided ribosomes, recognizing the similar composite binding site formed between the two ribosomes. In both cases, residues in the DxH/DLR and HGxG motifs are oriented towards the mRNA. In the case of SmrB, the DLH residues are involved in catalysis; in the case of MutS2, our data suggest that the DLR and HGxG sequences are required for high affinity binding to ribosomes but not for endonucleolytic cleavage. We note that the sucrose gradient sedimentation binding assay is a stringent test as evidenced by the fact that SMR domain mutants that fail to bind robustly still retain partial rescue activity. Ribosome binding is likely aided by auxiliary interactions of SmrB and MutS2 with the periphery of the collision interface, at sites that are accessible on all ribosomes, not only collided ones. For example, the interactions between the KOW domain of MutS2 and uS10 may be sufficient for

partial activity even without the SMR domain. Most notably, as revealed by cryo-EM structures, the orientations of the SMR domains of SmrB and MutS2 are completely different, consistent with the difference in terms of catalytic activity of the two proteins.

Apparently, although SMR domains act as conserved ribosome collisions sensors in bacteria, not all have nuclease activity. We do not see any evidence that MutS2 targets mRNAs encoding stalling sequences for degradation as SmrB does so effectively in *E. coli*. Consistent with this, although the DxH residues associated with SmrB endonuclease activity in proteobacteria are also conserved in Bacteroidetes proteins with the KOW-SMR architecture, they are only rarely present in the proteins with the MutS2 architecture. Substitution of the histidine in the DxH motif required for metal-independent catalysis appears to be a repeated theme throughout the SMR family, occurring several times in various lineages. The SmrA proteins in gammaproteobacteria, for example, which are paralogs of SmrB, wholly lack the residues necessary for nuclease activity. In plants, SMR domains display a diversity of active sites, with some retaining the DxH, others containing the same DxR motif reported here for MutS2, and still others with further substitutions of these residues[35].

Based on the growing evidence for the role of SMR domains in sensing ribosome collisions, we propose that SMR-domain proteins participate in at least two pathways. The active versions, like SmrB, Cue2, and Nonu-1, work via mRNA cleavage at collisions. In bacteria, cleavage leads to ribosome rescue by the tmRNA pathway; in eukaryotes, the active SMR versions likely function along with the exosomal mRNA degradation system conserved in the archaeo-eukaryotic lineage. In contrast, the inactive versions, like MutS2, are likely to depend on ribosome-splitting pathways coupled with the ancient RqcH/Rqc2 pathway that was present in the last universal common ancestor. While MutS2 carries its own ABC ATPase domain, critical for ribosome splitting, in eukaryotes the inactive SMR domains could function along with related but distinct ribosome-splitting enzymes of the translation factor ABC ATPase clade (e.g. Rli1 in yeast and ABCE1 in humans). Thus, the SMR domains parallel the evolution of the RNase H-fold release factor (eRF1) family[44], which also features both catalytically active versions involved in release of the polypeptide from the tRNA (e.g. eRF1) and inactive versions that separate ribosomal subunits (e.g. Dom34 in yeast and PELO in humans).

Materials and Methods

Bacterial strains and plasmids

A list of strains and plasmids and the details of their construction are given in Table S1. Knockout strains were obtained from the Bacillus Genetic Stock Center (BGSC)[45]. The reporter constructs and CamR marker were introduced into the *amyE* locus through recombination[46] and verified by PCR and Sanger sequencing. All reporter constructs were expressed from a P_{veg} promoter and a strong ribosome binding site (RBS)[47]. N-terminal Flag-tagged versions of MutS2 with a spectinomycin resistance marker were introduced into *ΔmutS2* cells into the *thrC* locus with the endogenous *mutS2* 5' UTR and terminator by recombination[46] and confirmed by PCR and Sanger sequencing.

Spotting Assays

Cells were grown overnight at 37 °C in liquid LB. The overnight cultures were diluted to prepare fivefold serial dilutions starting from OD_{600} = 0.005. Subsequently, 1.5 μl of the diluted cultures was spotted on LB plates with or without various antibiotics. Plates were then incubated at 37 °C.

Polysome profiling

B. subtilis cells were cultured at 37 °C in 500 mL of LB to OD_{600} = 0.45, at which point the cells were treated for 5 min with antibiotics at the concentrations indicated in the figures. Cells were harvested by filtration using a Kontes 99-mm filtration apparatus with a 0.45 μm nitrocellulose filter (Whatman) and flash frozen in liquid nitrogen. Cells were then lysed in lysis buffer (20 mM Tris pH 8.0, 10 mM $MgCl_2$, 100 mM NH_4Cl, 5mM $CaCl_2$, 0.4% Triton X-100, 0.1% NP-40, 1mM chloramphenicol, 100 U ml^{-1} DNase I) using a Spex 6875D freezer mill with six cycles of 1 min grinding at 6 Hz and 1 min cooling. Lysates were centrifuged at 20,000 x g for 10 min at 4 °C to pellet cell debris. Samples that were subjected to RNase A digestion to detect nuclease-resistant disomes were incubated for 1 h at 25 °C with 15 μl of RNase A (1:1,000 dilution) then treated with 6 μl of SUPERase-In RNase Inhibitor (Thermo Fisher). Sucrose gradients of 10-50% were prepared using a Gradient Master 108 (Biocomp) with gradient buffer (20 mM Tris pH 8.0, 10 mM $MgCl_2$, 100 mM NH_4Cl, 2 mM DTT). Then, 15 – 30 AU of lysate was loaded on top of the sucrose gradient and centrifuged in an SW 41 rotor at 35,000 r.p.m. for 2.5 h at 4 °C. Fractionation was performed on a Piston Gradients Fractionator (Biocomp). To process each fraction for western blots, proteins were precipitated in 10% TCA. After pelleting, pellets were washed twice in ice-cold acetone and vacuum dried for 5 min. Finally, we resuspended each pellet in 6X loading dye and neutralized with Tris-HCl pH 7.5. Samples were probed on western blots using an anti-Flag-HRP antibody (1:2,000 dilution) and detected using SuperSignal West Femto Maximum Sensitivity Substrate (Thermo Fisher) and visualized using the ChemiDoc Omaging System (Biorad).

Western Blots

Cells were grown in LB with appropriate antibiotics to OD_{600} ~ 1. 1 mL of culture was harvested by centrifugation, resuspended in lysis buffer (100 mM NaCl, 50 mM EDTA) with 7 µl of 10 mg ml^{-1} lysozyme and incubated at 37 °C for 30 min. After 40 µl of 20% sarkosyl was added, the samples were incubated for 5 min at 37 °C. Then, 6X loading dye (250 mM Tris pH 6.8, 20% glycerol, 30% β-mercaptoethanol, 10% SDS, saturated bromophenol blue) was added and the lysate was denatured at 90 °C for 10 min. Protein was separated on either a 4-12% or 12% Criterion XT Bis-Tris protein gel (Bio-Rad) with XT-MES buffer and transferred to polyvinylidene membranes using the Trans-Blot Turbo Transfer system (Bio-Rad). Membranes were blocked in 5% milk for 1 h at room temperature, washed and then probed with antibodies diluted in TBS-Tween at the following dilutions: anti-NanoLuc, 1:2,000 (Promega); anti-FtsZ, 1:2,000 (Sigma); anti-mouse-HRP, 1:4,000 (Thermo Fisher); anti-rabbit-HRP, 1:4,000 (Santa Cruz Biotechnologies). Chemiluminescent signals from HRP were detected using SuperSignal West Pico PLUS Chemiluminescent Substrate (Thermo Fisher) or SuperSignal West Femto Maximum Sensitivity Substrate (Thermo Fisher) and were visualized using the ChemiDoc Imaging System (Bio-Rad).

Northern Blots

Cells were grown in LB to OD_{600} = 0.5, an equal volume of ice-cold methanol was added, and the samples were harvested by centrifugation. Pellets were frozen on dry ice and stored at -80 °C. Pellets were then thawed on ice and resuspended in lysis buffer (30 mM Tris pH 8.0, 10 mM EDTA). An equal amount of lysis buffer with 10 mg ml^{-1} lysozyme was added to the lysates and incubated at 37 °C shaking at 1000 rpm. for 30 min. RNA was extracted twice with phenol (pH 4.5) first at 65 °C and then at room temperature, followed by chloroform extraction. The RNA in the aqueous layer was precipitated with isopropanol and 0.3 M sodium acetate (pH 5.5), washed with 80% ethanol, and resuspended in water. The purified RNA was separate on a 1.2% agarose-formaldehyde denaturing gel and was then transferred to a nylon membrane (Hybond-N+, Cytvia) in 10X SSC buffer using a model 785 vacuum blotter (Bio-Rad). RNA was cross-linked to the membrane using an ultraviolet (UV) cross-linker (Stratgen). Pre-hybridization and hybridization were performed in PerfectHyb Plus Hybridization Buffer (Sigma). The RNA was probed with 50-150 nM 5'-digoxigenin-labeled DNA oligonucleotides (IDT). Digoxigenin was detected with anti-digoxigenin-AP antibodies diluted 1:500 – 1:1000 (Sigma). Chemiluminescent signals from alkaline phosphatase were detected with CDP-star (Sigma) and were visualized using the ChemiDoc Imaging System (Bio-Rad).

MS analysis of tagging sites on the reporter protein

Strains expressing the ApdA reporter were grown in 100 mL of LB with 20 µM bortezomib until OD_{600} = 0.5 and harvested by centrifugation. The pellet was frozen at -80 °C and thawed in 2X CellLytic B cell lysis reagent (Sigma) and 0.2 mg mL^{-1} lysozyme for 10 minutes. The lysate was clarified by centrifugation for 30 minutes at 20,000 x g at 4 °C. 50 µL of Strep-tactin Sepharose beads (IBA) were added to the supernatant and samples were incubated at 4 °C for 1 h. The beads were washed four times with IP wash buffer (20 mM Tris pH 8.0, 100 mM NH_4Cl, 0.4% Triton X-

100, 0.1% NP-40) for 5 min at 4 °C. Protein was eluted from the beads by shaking at 4 °C in elution buffer (20 mM Tris pH 8.0, 100 mM NH_4Cl, 5 mM desthiobiotin) for 1 h. Then, 36 µl of immunoprecipitated sample was reduced with 100 mM DTT in 100 mM triethylammonium bicarbonate (TEAB) buffer at 58 °C for 55 min and then the pH was adjusted to 8.0. The samples were alkylated with 200 mM iodoacetamide in 100 mM TEAB buffer in the dark at room temperature for 15 min. Proteins were pelleted and resuspended in 50 mM TEAB and proteolyzed with 15 ng μL^{-1} of LysC (Wyco) at 37 °C overnight. Peptides were desalted on Oasis u-HLB plates (Waters), eluted with 60% acetonitrile (ACN) / 0.1% trifluoracetic acid (TFA), dried and reconstituted with 2% ACN / 0.1% formic acid.

LC-MS/MS analysis: Desalted peptides cleaved by LysC were analyzed by LC-MS/MS. Then peptides were separated reverse-phase chromatography (2 – 90% ACN/0.1% formic acid gradient over 63 min at a rate of 300 nl min^{-1}) on a 75 µm x 150 mm ReproSIL-Pur-120-C18-AQ column (Dr. Albin Maisch, Germany) using the nano-EasyLC 1200 system (Thermo). Eluting peptides were sprayed into an Orbitrap-Lumos_ETD mass spectrometer through a 1 µm emitter tip (New Objective) at 2.4 kV. Scans were acquired within 350 – 1600 Da *m/z* targeting the truncated reporter with 15 s dynamic exclusion. Precursor ions were individually isolated 0.7 Da and were fragmented (MS/MS) using an HCD activation collision energy of 30. Precursor (fragment) ions were analysed at a resolution of 200 Da of 120,000 with the following parameters: max injection time (IT), 100 ms (resolution of 30,000) in three cycles. The MS/MS spectra were processed with Proteome Discover v2.4 (Thermo Fisher) and were analyzed with Mascot v.2.8.0 (Matrix Science) using RefSeq2021_204_Bacillus.S and a database with peptides from the NanoLuc-BleR reporter protein. Peptide identifications from Mascot searches were processed within the Proteome Discoverer-Percolator to identify peptides with a confidence threshold of a 5% false discovery rate, as determined by an auto-concatenated decoy database search.

Purification of MutS2

N-terminally His-tagged versions of MutS2 were expressed from pET-24d(+) plasmids in BL21(DE3) *E. coli* cells. Cells were grown in 9 L LB medium to approximately OD_{600} = 2.5 and MutS2 expression was induced with IPTG (1 mM). Cells were harvested by centrifugation and resuspended in 30 mL lysis buffer (20 mM Hepes pH 7.5, 95 mM KCl, 5 mM NH_4Cl, 10 mM $Mg(OAc)_2$, 1 mM DTT, protease inhibitor (Roche)), then lysed using a microfluidizer (15k psi, H10Z, Microfluidics). Lysates were cleared by centrifugation (16,000 rpm, 20 min, 4 °C, Sorvall SS-34 rotor). Cleared lysates were applied to 3 mL TALON Metal Affinity Resin (Takara) and incubated for 30 minutes at 4 °C. The resin was washed with 40 mL each of wash buffer (50 mM Hepes pH 7.5, 225 mM NH_4Cl, 20 mM $MgCl_2$, 0.1 mM PMSF, 5% Glycerol, 1 mM DTT, 20 mM imidazole, 0.4% Triton X-100, protease inhibitor), wash buffer with 1 M KCl, and wash buffer without imidazole or Triton X-100, sequentially. The protein was eluted by incubation with 5 mL wash buffer with 150 mM imidazole, followed by a second elution with 200 mM imidazole. Elution fractions were analysed by Superdex 200 gel filtration and fractions containing pure MutS2 protein were pooled, concentrated using an Amicon 50kDa MWCO concentrator, and used for the cryo-EM and subunit splitting experiments.

Cryo-EM analyses

Sample preparation: His-MutS2 WT was added to purified disomes from *B. subtilis* in 10-fold excess in reaction buffer (50 mM HEPES/KOH pH 7.5, 75 mM KOAc, 5 mM $Mg(OAc)_2$, 1.2 mM DTT, 45 mM NH_4Cl, 4 mM $MgCl_2$, 1% glycerol, 1 mM $MnCl_2$, 1 mM AMP-PNP) and the mixture was incubated at 30 °C for 1 h. Following this, the sample was directly vitrified for cryo-EM by plunge-freezing using a Vitrobot Mark IV (FEI Company/Thermo Fisher) with an incubation time of 45 s and blotting for 2.5 s at 4 °C and a humidity of 95%.

Data collection: Data were collected on a Titan Krios G3 (Thermo Fisher) equipped with a K2 direct detector (Gatan) at 300 keV using the semi-automated data acquisition software EPU (Thermo Fisher). 40 frames with a dose of 1.09 $^{e-}/Å^2$ per frame were collected in a defocus range of -0.4 to -3.5 µm. Magnification settings resulted in a pixel size of 1.045 Å/pixel. Frame alignment was executed with MotionCor2 (56) and the estimation of the contrast transfer function (CTF) was performed with Gctf (57).

Processing: After manual screening of micrographs, 5,784 were selected for particle picking using Gautomatch (http://www.mrclmb.cam.ac.uk/kzhang/) with a set of reference images generated from a *B. subtilis* disome model (28). After 2D classification in Relion 3.1, 96,978 particles representing collided disomes were selected for further processing. After several rounds of 3D classification and refinement in Relion in order to remove classes without a rigid disome interface or density for the mRNA in the inter-ribosomal space, a class of 15,239 particles displaying a significant extra density next to the inter-ribosomal mRNA were selected for high-resolution refinement in CryoSPARC. Homogenous refinement and focused refinement yielded a final reconstruction of the collided disome bound by the MutS2 KOW and SMR domains at an overall resolution of 4.2 Å.

MutS2 model building: In order to verify the identification of the extra densities observed in the reconstruction of the *B. subtilis* disome as MutS2, structures of the SMR and KOW domains of MutS2 as predicted by Alphafold 2 were fitted as rigid bodies into the densities in ChimeraX 1.0. A model of the collided disome bound by MutS2 was generated by adding these models to the model of a collided *B. subtilis* disome from (28) and refining the resulting model in Phenix 1.20.1 after minor adjustments based on the experimental data.

In vitro splitting assays

Purified versions (WT, SMR domain mutants, Walker A and Walker B mutants) of the MutS2 protein were added to purified disomes from *B. subtilis* in 10-fold excess in reaction buffer (50 mM HEPES/KOH pH 7.5, 75 mM KOAc, 5 mM $Mg(OAc)_2$, 1.2 mM DTT, 45 mM NH_4Cl, 4 mM $MgCl_2$, 1% glycerol, 1 mM $MnCl_2$) together with 1 mM ATP, 1 mM AMP-PNP, or no additional nucleotides and the mixture was incubated at 30 °C for 1 h. Samples were then applied to 10%-50% continuous sucrose density gradients (50 mM HEPES/KOH pH 7.5, 100 mM KOAc, 5 mM $Mg(OAc)_2$, 1 mM DTT). The gradients were centrifuged in an SW40Ti rotor (Beckman Coulter) at 202,408 x g

for 150 min and fractionated using a BioComp Gradient Station while UV absorption at 260 nm was recorded using a Triax Flow Cell FC-2.

Acknowledgments

The authors thank Bob Cole and Tatiana Boronina at JHMI in the Mass Spectrometry and Proteomics Facility and Joanna Musial for excellent technical assistance. This work was supported by NIH grant GM136960 (ARB), HHMI (RG), the German Research Council (TRR174) (RB), and by the Intramural Research Program of the National Library of Medicine at the NIH (AMB and LA).

Conflict of interest

The authors declare that there are no competing interests.

Data availability

Cryo-EM volumes and molecular models have been deposited at the Electron Microscopy Data Bank and Protein Data Bank with accession codes EMD-XXXX (maps) and PDB-YYYY (stalled 70S) PDB-ZZZZ (collided 70S).

References

1. Yan LL, Zaher HS. How do cells cope with RNA damage and its consequences? J Biol Chem. 2019 Oct 11;294(41):15158–15171.

2. Thomas EN, Kim KQ, McHugh EP, Marcinkiewicz T, Zaher HS. Alkylative damage of mRNA leads to ribosome stalling and rescue by trans translation in bacteria. eLife. 2020 Sep 17;9:e61984.

3. Roche ED, Sauer RT. SsrA-mediated peptide tagging caused by rare codons and tRNA scarcity. EMBO J. 1999 Aug 16;18(16):4579–4589.

4. Ude S, Lassak J, Starosta AL, Kraxenberger T, Wilson DN, Jung K. Translation Elongation Factor EF-P Alleviates Ribosome Stalling at Polyproline Stretches. Science. 2013 Jan 4;339(6115):82–85.

5. Doerfel LK, Wohlgemuth I, Kothe C, Peske F, Urlaub H, Rodnina MV. EF-P Is Essential for Rapid Synthesis of Proteins Containing Consecutive Proline Residues. Science. 2013 Jan 4;339(6115):85–88.

6. Woolstenhulme CJ, Parajuli S, Healey DW, Valverde DP, Petersen EN, Starosta AL, Guydosh NR, Johnson WE, Wilson DN, Buskirk AR. Nascent peptides that block protein synthesis in bacteria. Proc Natl Acad Sci U S A. 2013 Mar 5;110(10):E878-887.

7. Nakatogawa H, Ito K. The Ribosomal Exit Tunnel Functions as a Discriminating Gate. Cell. 2002 Mar;108(5):629–636.

8. Su T, Kudva R, Becker T, Buschauer R, Komar T, Berninghausen O, von Heijne G, Cheng J, Beckmann R. Structural basis of L -tryptophan-dependent inhibition of release factor 2 by the TnaC arrest peptide. Nucleic Acids Res. 2021 Sep 20;49(16):9539–9547.

9. Gong F, Yanofsky C. Instruction of translating ribosome by nascent peptide. Science. 2002 Sep 13;297(5588):1864–1867.

10. Bhushan S, Hoffmann T, Seidelt B, Frauenfeld J, Mielke T, Berninghausen O, Wilson DN, Beckmann R. SecM-stalled ribosomes adopt an altered geometry at the peptidyl transferase center. PLoS Biol. 2011 Jan 18;9(1):e1000581.

11. Polikanov YS, Aleksashin NA, Beckert B, Wilson DN. The Mechanisms of Action of Ribosome-Targeting Peptide Antibiotics. Front Mol Biosci. 2018;5:48.

12. Wilson DN. The A-Z of bacterial translation inhibitors. Crit Rev Biochem Mol Biol. 2009;44(6):393–433.

13. Buskirk AR, Green R. Ribosome pausing, arrest and rescue in bacteria and eukaryotes. Philos Trans R Soc B Biol Sci. 2017 Mar 19;372(1716):20160183.

14. Ivanova N, Pavlov MY, Felden B, Ehrenberg M. Ribosome Rescue by tmRNA Requires Truncated mRNAs. J Mol Biol. 2004 Apr;338(1):33–41.

15. Neubauer C, Gillet R, Kelley AC, Ramakrishnan V. Decoding in the absence of a codon by tmRNA and SmpB in the ribosome. Science. 2012 Mar 16;335(6074):1366–1369.

16. Keiler KC, Waller PRH, Sauer RT. Role of a Peptide Tagging System in Degradation of Proteins Synthesized from Damaged Messenger RNA. Science. 1996 Feb 16;271(5251):990–993.

17. Garza-Sánchez F, Schaub RE, Janssen BD, Hayes CS. tmRNA regulates synthesis of the ArfA ribosome rescue factor: tmRNA regulates ArfA synthesis. Mol Microbiol. 2011 Jun;80(5):1204–1219.

18. Chadani Y, Ono K, Ozawa S ichiro, Takahashi Y, Takai K, Nanamiya H, Tozawa Y, Kutsukake K, Abo T. Ribosome rescue by Escherichia coli ArfA (YhdL) in the absence of trans-translation system: Ribosome rescue by E. coli ArfA (YhdL). Mol Microbiol. 2010 Nov;78(4):796–808.

19. Shimokawa-Chiba N, Müller C, Fujiwara K, Beckert B, Ito K, Wilson DN, Chiba S. Release factor-dependent ribosome rescue by BrfA in the Gram-positive bacterium Bacillus subtilis. Nat Commun. 2019 Dec;10(1):5397.

20. Matsuo Y, Ikeuchi K, Saeki Y, Iwasaki S, Schmidt C, Udagawa T, Sato F, Tsuchiya H, Becker T, Tanaka K, Ingolia NT, Beckmann R, Inada T. Ubiquitination of stalled ribosome triggers ribosome-associated quality control. Nat Commun. 2017 Dec;8(1):159.

21. Matsuo Y, Tesina P, Nakajima S, Mizuno M, Endo A, Buschauer R, Cheng J, Shounai O, Ikeuchi K, Saeki Y, Becker T, Beckmann R, Inada T. RQT complex dissociates ribosomes collided on endogenous RQC substrate SDD1. Nat Struct Mol Biol. 2020 Apr;27(4):323–332.

22. Filbeck S, Cerullo F, Pfeffer S, Joazeiro CAP. Ribosome-associated quality-control mechanisms from bacteria to humans. Mol Cell. 2022 Apr;82(8):1451–1466.

23. Kostova KK, Hickey KL, Osuna BA, Hussmann JA, Frost A, Weinberg DE, Weissman JS. CAT-tailing as a fail-safe mechanism for efficient degradation of stalled nascent polypeptides. Science. 2017 Jul 28;357(6349):414–417.

24. Shen PS, Park J, Qin Y, Li X, Parsawar K, Larson MH, Cox J, Cheng Y, Lambowitz AM, Weissman JS, Brandman O, Frost A. Protein synthesis. Rqc2p and 60S ribosomal subunits mediate mRNA-independent elongation of nascent chains. Science. 2015 Jan 2;347(6217):75–78.

25. Lytvynenko I, Paternoga H, Thrun A, Balke A, Müller TA, Chiang CH, Nagler K, Tsaprailis G, Anders S, Bischofs I, Maupin-Furlow JA, Spahn CMT, Joazeiro CAP. Alanine Tails Signal Proteolysis in Bacterial Ribosome-Associated Quality Control. Cell. 2019 Jun;178(1):76-90.e22.

26. Crowe-McAuliffe C, Takada H, Murina V, Polte C, Kasvandik S, Tenson T, Ignatova Z, Atkinson GC, Wilson DN, Hauryliuk V. Structural Basis for Bacterial Ribosome-Associated Quality Control by RqcH and RqcP. Mol Cell. 2021 Jan;81(1):115-126.e7.

27. Takada H, Crowe-McAuliffe C, Polte C, Sidorova ZY, Murina V, Atkinson GC, Konevega AL, Ignatova Z, Wilson DN, Hauryliuk V. RqcH and RqcP catalyze processive poly-alanine synthesis in a reconstituted ribosome-associated quality control system. Nucleic Acids Res. 2021 Aug 20;49(14):8355–8369.

28. Saito K, Kratzat H, Campbell A, Buschauer R, Burroughs AM, Berninghausen O, Aravind L, Green R, Beckmann R, Buskirk AR. Ribosome collisions induce mRNA cleavage and ribosome rescue in bacteria. Nature. 2022 Mar 17;603(7901):503–508.

29. Ferrin MA, Subramaniam AR. Kinetic modeling predicts a stimulatory role for ribosome collisions at elongation stall sites in bacteria. eLife. 2017 May 12;6:e23629.

30. Simms CL, Yan LL, Zaher HS. Ribosome Collision Is Critical for Quality Control during No-Go Decay. Mol Cell. 2017 Oct;68(2):361-373.e5.

31. Juszkiewicz S, Chandrasekaran V, Lin Z, Kraatz S, Ramakrishnan V, Hegde RS. ZNF598 Is a Quality Control Sensor of Collided Ribosomes. Mol Cell. 2018 Nov;72(3):469-481.e7.

32. Ikeuchi K, Tesina P, Matsuo Y, Sugiyama T, Cheng J, Saeki Y, Tanaka K, Becker T, Beckmann R, Inada T. Collided ribosomes form a unique structural interface to induce Hel2-driven quality control pathways. EMBO J. 2019 Mar; 38(5).

33. Cerullo F, Filbeck S, Patil PR, Hung HC, Xu H, Vornberger J, Hofer FW, Schmitt J, Kramer G, Bukau B, Hofmann K, Pfeffer S, Joazeiro CAP. Bacterial ribosome collision sensing by a MutS DNA repair ATPase paralogue. Nature. 2022 Mar 17;603(7901):509–514.

34. D'Orazio KN, Wu CCC, Sinha N, Loll-Krippleber R, Brown GW, Green R. The endonuclease Cue2 cleaves mRNAs at stalled ribosomes during No Go Decay. eLife. 2019 Jun 20;8:e49117.

35. Glover ML, Burroughs AM, Monem PC, Egelhofer TA, Pule MN, Aravind L, Arribere JA. NONU-1 Encodes a Conserved Endonuclease Required for mRNA Translation Surveillance. Cell Rep. 2020 Mar 31;30(13):4321-4331.e4.

36. Lamers MH, Perrakis A, Enzlin JH, Winterwerp HH, de Wind N, Sixma TK. The crystal structure of DNA mismatch repair protein MutS binding to a G x T mismatch. Nature. 2000 Oct 12;407(6805):711–717.

37. Saxena S, Myka KK, Washburn R, Costantino N, Court DL, Gottesman ME. Escherichia coli transcription factor NusG binds to 70S ribosomes. Mol Microbiol. 2018 Jun;108(5):495–504.

38. Zhou W, Lu Q, Li Q, Wang L, Ding S, Zhang A, Wen X, Zhang L, Lu C. PPR-SMR protein SOT1 has RNA endonuclease activity. Proc Natl Acad Sci U S A. 2017 Feb 21;114(8):E1554–E1563.

39. Chiba S, Ito K. Multisite Ribosomal Stalling: A Unique Mode of Regulatory Nascent Chain Action Revealed for MifM. Mol Cell. 2012 Sep;47(6):863–872.

40. Jumper J, Evans R, Pritzel A, Green T, Figurnov M, Ronneberger O, Tunyasuvunakool K, Bates R, Žídek A, Potapenko A, Bridgland A, Meyer C, Kohl SAA, Ballard AJ, Cowie A, Romera-Paredes B, Nikolov S, Jain R, Adler J, Back T, Petersen S, Reiman D, Clancy E, Zielinski M, Steinegger M, Pacholska M, Berghammer T, Bodenstein S, Silver D, Vinyals O, Senior AW, Kavukcuoglu K, Kohli P, Hassabis D. Highly accurate protein structure prediction with AlphaFold. Nature. 2021 Aug;596(7873):583–589.

41. Sakiyama K, Shimokawa-Chiba N, Fujiwara K, Chiba S. Search for translation arrest peptides encoded upstream of genes for components of protein localization pathways. Nucleic Acids Res. 2021 Feb 22;49(3):1550–1566.

42. Trinquier A, Durand S, Braun F, Condon C. Regulation of RNA processing and degradation in bacteria. Biochim Biophys Acta BBA - Gene Regul Mech. 2020 May;1863(5):194505.

43. Fei X, Bell TA, Barkow SR, Baker TA, Sauer RT. Structural basis of ClpXP recognition and unfolding of ssrA-tagged substrates. eLife. 2020 Oct 22;9:e61496.

44. Burroughs AM, Aravind L. The Origin and Evolution of Release Factors: Implications for Translation Termination, Ribosome Rescue, and Quality Control Pathways. Int J Mol Sci. 2019 Apr 23;20(8):1981.

45. Koo BM, Kritikos G, Farelli JD, Todor H, Tong K, Kimsey H, Wapinski I, Galardini M, Cabal A, Peters JM, Hachmann AB, Rudner DZ, Allen KN, Typas A, Gross CA. Construction and Analysis of Two Genome-Scale Deletion Libraries for Bacillus subtilis. Cell Syst. 2017 Mar;4(3):291-305.e7.

46. Guérout-Fleury AM, Frandsen N, Stragier P. Plasmids for ectopic integration in Bacillus subtilis. Gene. 1996 Nov 21;180(1–2):57–61.

47. Guiziou S, Sauveplane V, Chang HJ, Clerté C, Declerck N, Jules M, Bonnet J. A part toolbox to tune genetic expression in *Bacillus subtilis*. Nucleic Acids Res. 2016 Jul 8;gkw624.

Supplemental Figures

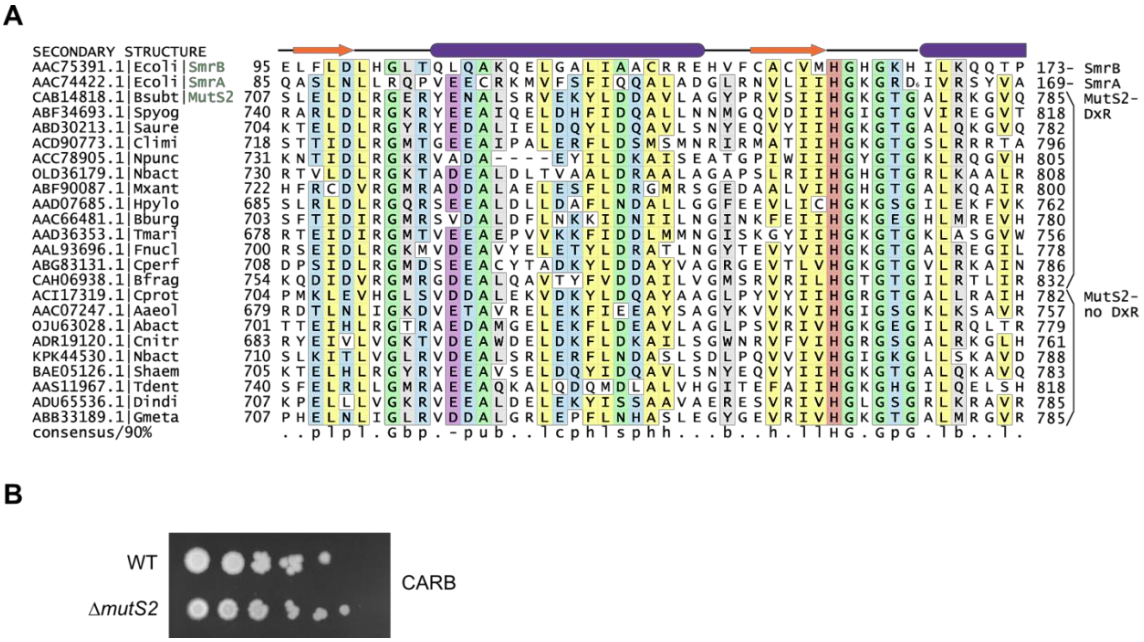

Figure S1. MutS2 SMR domain architecture. (A) Multiple alignment of the conserved residues in the SMR domain of SMR proteins from different bacteria. Columns in the alignment are shaded and labeled according to biochemical character: -, negatively charged in purple; c, charged in blue; h, hydrophobic in yellow; p, polar in blue; l, aliphatic in yellow; b, big in gray; s, small in green; u, tiny in green; G, glycine in green; H, histidine in red. Sequences are labeled with NCBI accession number and organism abbreviation. Secondary structure provided at top of alignment. Numbers to left and right of alignment denote positioning of the region. **(B)** Spotting assay showing that *ΔmutS2* cells are not hypersensitive to carbenicillin (0.05 μg/mL).

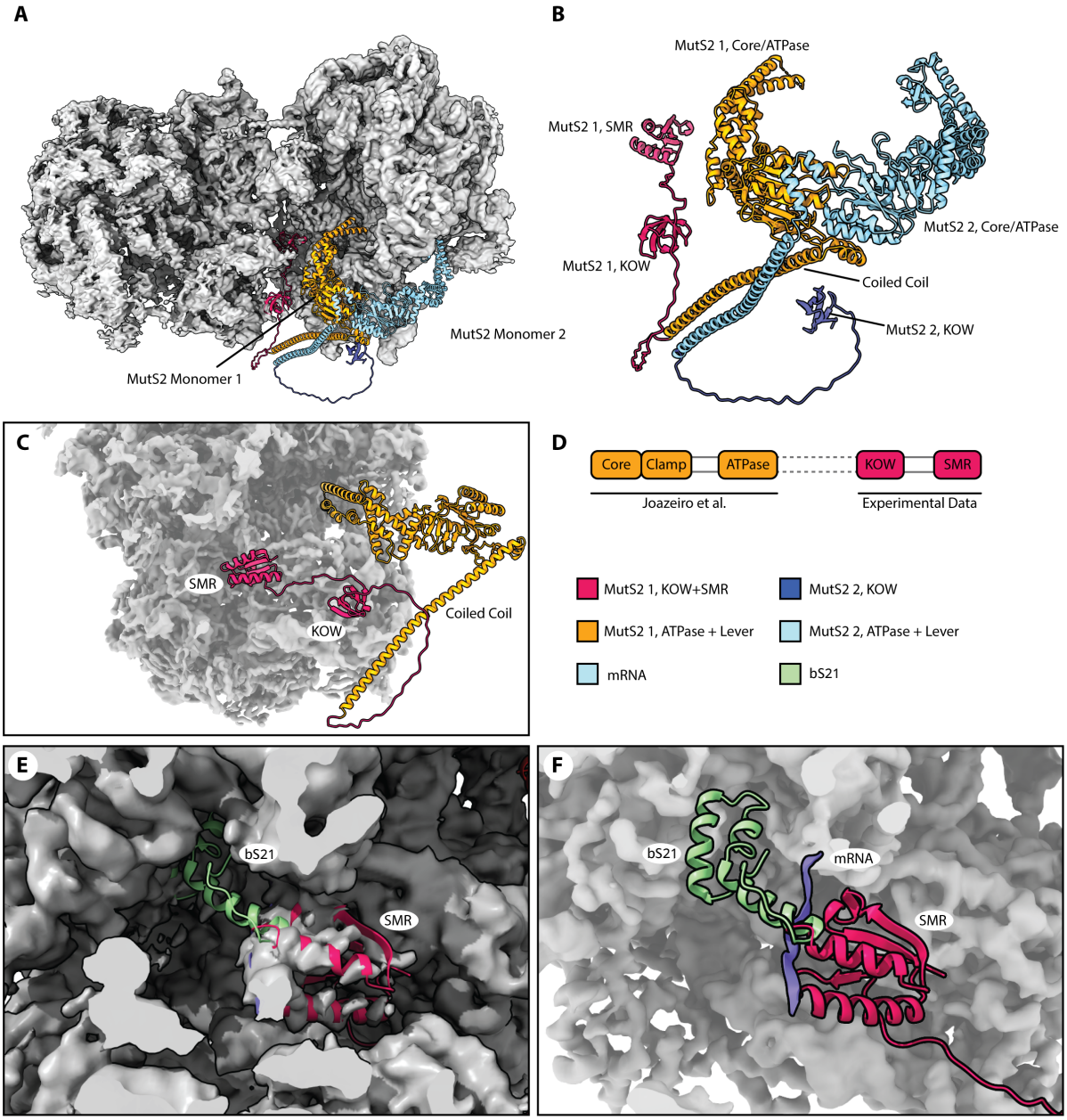

Figure S2. MutS2 KOW and SMR domain bind the ribosome in a manner congruent with previous studies on the MutS2 Core/ATPase domains. (A) Experimental cryo-EM map (grey) and model of the MutS2 dimer binding a collided disome in B. subtilis. The SMR and KOW domains of MutS2 monomer 1 (red) as well as the KOW domain of MutS2 monomer 2 (violet) recruit the MutS2 are visible in the cryo-EM reconstruction. The Core/ATPase domains are not visible in the reconstruction, but the structure as published by Joazeiro et al. (monomer 1: yellow, monomer 2: light blue) is congruent with the experimental observations. **(B)** Isolated view of the composite structure of the MutS2 dimer: The length of the flexible loop between coiled coil and KOW domains does not allow a stringent assignment of either KOW domain to either monomer from the Joazeiro et al. structure, hence the assignment shown here was chosen arbitrarily. **(C)** Side view of MutS2 monomer 1 engaged with the stalled ribosome. **(D)** Schematic representation of the composite structure of MutS2 shown in (A) and (B). **(E)** Fit of the MutS2 monomer 1 SMR domain into the experimental density and comparison with the hypothetical location of bS21 as observed by Cerullo *et al*. In our experimental data, there is no evidence that bS21 is present in the MutS2-bound collided disomes. **(F)** Representation of the experimentally determined location of the MutS2 monomer 1 SMR domain and the hypothetical position of bS21. If bound to the ribosome as in Joazeiro et al., bS21 would clash with the observed conformation of MutS2 SMR next to the mRNA.

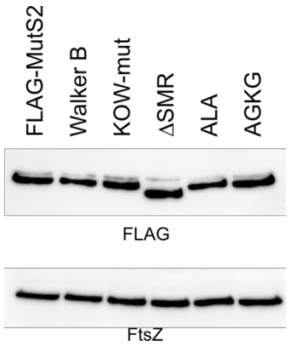

Figure S3. Expression levels of MutS2 constructs are not variable. Levels of FLAG-tagged constructs of MutS2 in *B. subtilis* cells were detected on a western blot using an anti-FLAG antibody. The FtsZ protein serves as a loading control.

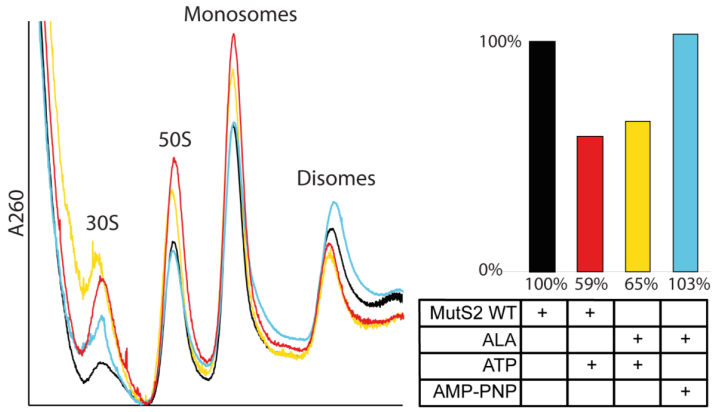

Figure S4. The DLR motif of MutS2 SMR domain is not essential for disome splitting. Left: UV chromatograms from sucrose gradient fractionation of disome splitting assays with MutS2 WT and MutS2 D_{711}LR to ALA mutant. Right: Relative abundance of disomes compared to total ribosomal fractions after splitting reaction, calculated from relative peak areas in the chromatograms. Purified *B. subtilis* disomes were used as input. The presence of the mutation has no effect on the efficiency of the splitting reaction either with or without hydrolysable ATP, indicating that the DLR motif of the SMR domain is not required for this process.